Energy Advances

PAPER

View Article Online
View Journal | View Issue

Cite this: *Energy Adv.*, 2024, 3, 592

Improved coulombic efficiency of single-flow, multiphase flow batteries *via* the use of strong-binding complexing agents†

Prakash Rewatkar, ‡*[ad] Mohamed Asarthen S, ‡[b] Robert Glouckhovski,[a] Ran Elazari[c] and Matthew E. Suss*[abd]

To support the energy transition, an inexpensive grid-scale energy storage device is needed to counteract the intermittency of renewable energy sources. Redox flow batteries (RFBs) offer the potential provide such storage, however, high capital costs have hampered market penetration. To reduce costs, single-flow configurations have been explored to eliminate expensive battery components and minimize balance of plant systems. Here, we report on a membraneless single-flow zinc–bromine battery leveraging a unique multiphase electrolyte. The use of such electrolyte emulsions, containing a bromine-poor aqueous phase and bromine-rich polybromide phase, have allowed for effective reactant separation in single-flow architectures, although at the cost of low cycling coulombic efficiency (CE). In this study, we show that significant improvements in CEs are possible when using strong-binding bromine complexing agents (BCAs) to form the polybromide phase. We compare battery performance when using widespread but relatively weak-binding BCA *N*-ethyl-*N*-methylpyrrolidinium bromide (MEP) or novel, stronger-binding 1-butyl-3-methylpyridinium bromide (3-MBPy). We characterize for the first time the *ex situ* viscosity, ionic conductivity and aqueous phase bromine concentration for such emulsive electrolytes, towards building a library of emulsive electrolyte properties. We show that the use of 3-MBPy significantly reduced zinc corrosion during cycling due to a reduced aqueous phase bromine concentration, enabling an up to 23% increase in CE when cycling at 30 mA cm^{-2}.

Received 22nd June 2023,
Accepted 8th January 2024

DOI: 10.1039/d3ya00293d

rsc.li/energy-advances

1. Introduction

Energy consumption has increased in nearly every sector of society during the last few decades. As a result, demand for virtually all fossil energy sources, including oil, petroleum coal, natural gas, nuclear energy, and renewables has increased.[1] Fossil fuels provide about 80% of the global energy demand, resulting in the energy sector accounting for two-thirds of global CO_2 emissions. The search for alternative clean and sustainable renewable energy sources has become a worldwide research trend, but its application has been impeded by the lack of cost-effective, large-scale energy storage solutions.[2] Flow-based electrochemical energy storage technology has emerged as a promising solution due to a relatively high energy conversion efficiency, geographic flexibility, and potentially long cycle life.[3] In general, the power rating of a redox flow battery (RFB) is determined by the active electrode area, while the battery capacity by the amount of electrolyte stored in external tanks, which allows for the unique spatial decoupling of energy storage and power delivery. Flow batteries can be classified according to their redox-active species, and highly investigated chemistries include all-vanadium,[4] Fe–Cr,[5] polysulfide/iodide,[6] polysulfide/bromide,[7] among others. Other chemistries, such as Zn–Br_2,[8] Zn–Ce[9] and lithium-based RFBs[10,11] are classified as hybrid RFBs as one of the electrodes performs metal deposition and dissolution within the battery during the charge–discharge cycle.[12]

Zinc–bromine flow batteries (ZBFB), have various advantages such as inexpensive and abundant reactants, fast electrochemical reactions without need for a metal catalyst, and a high theoretical energy density.[13] Typical ZBFBs contain one positive electrode for bromine reduction and oxidation and one negative zinc electrode, separated by an ion exchange membrane or non-selective separator enabling two flows, a negolyte

[a] *Faculty of Mechanical Engineering, Technion-Israel Institute of Technology, Haifa, 3200003, Israel. E-mail: prakash.r@campus.technion.ac.il, mesuss@technion.ac.il*
[b] *The Wolfson Department of Chemical Engineering, Technion-Israel Institute of Technology, Haifa, 3200003, Israel*
[c] *Israel Chemicals Limited (ICL), Israel*
[d] *The Nancy & Stephen Grand Technion Energy Program, Technion-Israel Institute of Technology, Haifa, 320003, Israel*

† Electronic supplementary information (ESI) available. See DOI: https://doi.org/10.1039/d3ya00293d

‡ These authors contributed equally to this work.

containing zinc ions and posolyte containing bromine and bromide ions.[14] The electrochemical reactions occurring include, at the negative electrode,

$$Zn \rightleftarrows Zn^{2+} + 2e^- \quad (E^0 = -0.76\ V\ vs.\ SHE)$$

at the positive electrode,

$$Br_2 + 2e^- \rightleftarrows 2Br^- \quad (E^0 = +1.08\ V\ vs.\ SHE)$$

yielding an overall reaction,

$$Zn + Br_2 \rightleftarrows Zn^{2+} + 2Br^- \quad (E = 1.84\ V)$$

During charging, zinc metal electrodeposition occurs at the negative electrode while bromine (Br_2) is evolved at the positive electrode from bromide ions. Much of the bromine complexes with Br^- in the electrolyte to create highly soluble Br_3^- or Br_5^- ions.[15] The ZBFB has a relatively high cell voltage for aqueous batteries of 1.84 V at standard conditions, which together with highly soluble reactants enables a practically achieved energy density of 60 W h L^{-1}.[16] As a result, it is one of the most widely investigated flow battery chemistries for large-scale energy storage.[17–19]

Since the first development of ZBFB, electrolyte additives have been used to reduce bromine vapor pressure, as bromine readily forms a corrosive gas at room temperature. These are often quaternary ammonium bromine complexation agents (BCAs) such as *N*-ethyl-*N*-methylpyrrolidinium (MEP), which is perhaps the most prominent BCA.[20–22] Complexation often leads to the formation of two phases, one aqueous which is bromine-poor but where the bromine is electrochemically active, and a denser polybromide phase which is bromine-rich but with reduced bromine activity.[22,23] More recently, several novel BCA molecules have been investigated, with spectroscopic experiments and density functional theory (DFT) applied to investigate the stability of BSA–polybromide complexes.[24] From the latter studies, it was found that weaker interionic bonds within the initial monobromide salt result in more stable higher-order BCA-polybromide complexes, and hence stronger bromine binding capability. The benchmark for selecting appropriate BCAs and their optimal performance is comprehensively discussed in Table S1 of the ESI.†

In conventional RFBs, the single most expensive component is often the ion-exchange membrane.[25,26] In addition to their high direct cost, such membranes significantly increase overall system cost indirectly through substantial resistive losses and potential fluid management issues caused by osmosis or electro-osmotic drag.[27] Numerous cell architectures have been investigated in order to enable membraneless operation, for example implementing a co-laminar electrolyte flow at high Peclet numbers to minimize reactant crossover between electrodes (anode and cathode).[28,29] Lai *et al.*[30] demonstrated a single flow ZBFB, where they incorporated microporous membrane and further added BCA in the electrolyte to limit the bromine cross-over thereby improving the energy density and CE. Thereafter, Biswas *et al.*[31] introduced a quiescent-electrolyte ZBFB achieving around 90% CE and 60% energy efficiency (EE) without any BCA or membrane. Lee *et al.* developed a membraneless flowless battery, building on the work of Biswas *et al.* with protonated, nitrogen-doped microporous carbons decorated on graphite felt for effective capture and conversion of bromine into polybromide.[32] Recently, Siyang *et al.*[33] developed a novel flowless membraneless ZBFB with high electrolyte concentration. Here they achieved CE of 98% and good stability of zinc anodes after more than 2500 cycles using LiCl as the additive without any BCA.

In order to explore low-cost single flow architectures, but allowing for effective reactant separation, recently flow batteries leveraging flowing emulsions as electrolytes have been proposed and explored. Amit *et al.*[34] reported a membrane-and-separator-free single-flow ZBFB leveraging an emulsion of a polybromide phase and an aqueous phase. The continuous aqueous phase was bromine-poor, while the bromine-rich polybromide phase was used at low volume fraction (1–5%) and was formed using MEP as the BCA. Bromine in the polybromide phase had a much-reduced electrochemical activity relative to that in the aqueous phase. While the concept enabled high current density of over 250 mA cm^{-2} and effective battery cycling, the achieved plating and cycling energy efficiencies were relatively low, as zinc corrosion by bromine during cycling was excessive. To further develop this concept, Ronen *et al.* in a series of papers established analytical current–voltage relationships for batteries leveraging emulsive electrolytes and uncovered that the effect of gravity on the polybromide phase plays a crucial role particularly at low electrolyte flowrate.[8,35] A separate effort to develop emulsions as flow battery electrolytes was detailed by Peng *et al.*[36] and Shen *et al.*[37] utilizing microemulsions of immiscible organic and aqueous solvents. In the latter system, organic molecules (ferrocene) soluble only in the organic phase (toluene/tween 20/1-butanol) was used as the redox-active species. This allows for the aqueous phase to serve as conductive pathways for ions, whereas the organic phase can contain a high-voltage redox couple.[36,37] Barth *et al.*[38] tested microemulsion electrolyte containing ferrocene as posolyte and menadione-SDS emulsion with 1-butanol and KNO_3 as negolyte in aqueous RFB. The recorded voltaic efficiency (VE) and energy efficiency were less than 60%, owing to high mass transport overpotentials, and capacity fading hindered the overall battery performance.

We here investigate the use of stronger-binding complexing agents than MEP in an effort to improve the coulombic and energy efficiencies of batteries leveraging a single flowing emulsion as electrolyte.[34] (Fig. 1) The present study examines and contrasts strong-binding 1-butyl-3-methylpyridinium bromide (3-MBPy) and relatively weak-binding MEP BCAs, both *ex situ* and within the single-flow ZBFB. Use of a stronger-binding complexing agent reduces the concentration of chemically active bromine in the aqueous phase, and so can potentially reduce zinc corrosion during battery cycling. To our knowledge, this is the first study on 3-MBPy for flow battery cycling. Several electrolyte parameters affecting battery performance, including viscosity, ionic conductivity, and equilibrium aqueous phase bromine concentration were measured *ex situ*. Battery charge–discharge measurements were used to quantify voltage, coulombic and energy efficiencies. It was found that

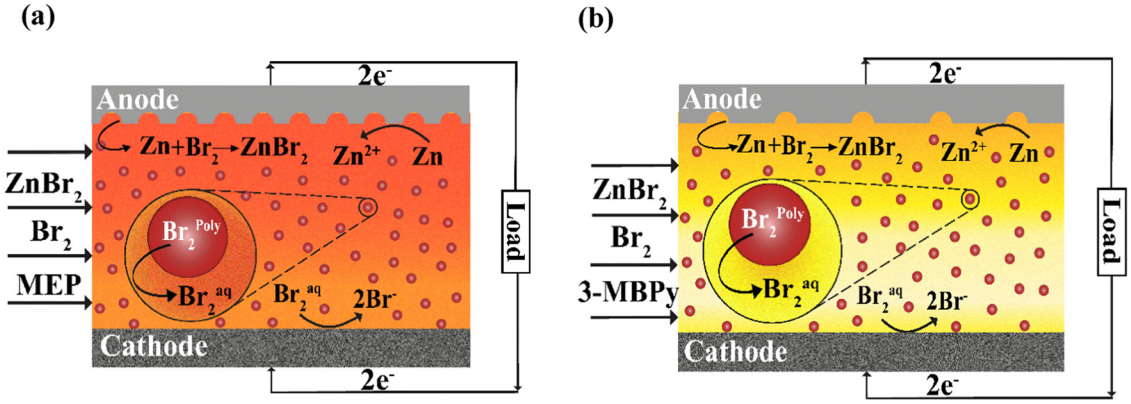

Fig. 1 Schematic of a single-flow battery with multiphase flow during discharge for the case of (a) a relatively weaker-binding BCA and (b) a stronger-binding BCA. (a) Use of a weaker-binding complexing agent, here MEP, leads to strong corrosion of the zinc anode by bromine in the continuous aqueous phase. (b) Use of strong-binding bromine complexing agent 3-MBPy, leads to reduced corrosion of the zinc anode due to lower bromine concentration in the aqueous phase.

use of the stronger-binding 3-MBPy BCA allowed for a 23% increase in coulombic efficiency as compared to cycling with MEP as BCA at otherwise identical conditions. These results demonstrate that the use of strong-binding BCAs is highly promising to enable improved performance from single-flow batteries leveraging multiphase flow electrolytes.

2. Experimental section

The battery consisted of endplates, current collectors and gaskets. Endplates and current collectors were milled using a rapid prototyping CNC milling machine (Roland DGA corporation, MDX 540, USA). Impervious graphite was used for the anode current collector (zinc electrode), and isomolded graphite served as the cathode (bromine electrode, GraphiteStore.com, Inc., USA), both 3 mm thick. Zinc metal was not inserted into the cell assembly, rather the zinc layer was electrodeposited *in situ* during cell charging. Prior to each experiment, the carbon current collectors were polished using a 0.05 μm polishing suspension (MasterPrep, Buehler, IL, USA) on a polishing cloth (Galaxy, Sigma). Endplates were 15 mm thick and fabricated from PVDF. A 2 mm thick gasket made of Viton rubber served as the flow channel, with an active area of 11.2 cm^2 cut into the gasket. PTFE gaskets (Gore® GR sheet Gasketing, 1.5 mm and Leader Gasket, Cipperlon 2130, 0.5 mm) were used to seal layers of the RFB prototype and were cut using laser ablation (VLS 3.6W, Universal laser system, USA). The cell was assembled using twelve M4, 60 mm long stainless-steel bolts wrapped with plastic heat shrink tubing to prevent internal short circuiting. The overall appearance of all fabricated components and assembly is depicted in Fig. 2a *via* an exploded view.

Electrolytes consisted of zinc bromide salt ($ZnBr_2$, 98% purity, Alfa Aesar, MA, USA), bromine (Br_2, Emsure, Merck, Germany), and complexing agents of either *N*-ethyl-*N*-methylpyrrolidinium bromide (MEP) or 1-butyl-3-methylpyridinium bromide (3-MBPy) supplied by ICL group Ltd, TLV, Israel. To prepare the electrolyte, 2 M $ZnBr_2$ salt was dissolved in DI

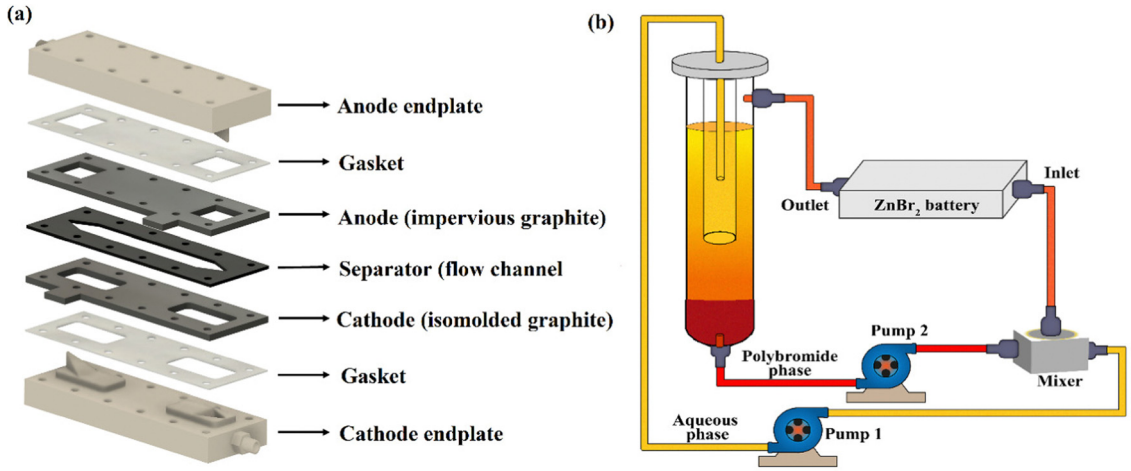

Fig. 2 (a) Exploded view schematic of prototype flow battery components, and (b) schematic of the experimental setup used to deliver the emulsive electrolyte to the battery prototype.

water, then 0.5 M MEP or 3-MBPy was added. Following that, 0.5 M Br_2 was added to the same well-mixed solution. The resultant solution was mixed thoroughly using orbital shaker incubator (TOU-50 N, MRC, Israel) at room temperature for 12 hours at 250 rpm. Afterwards, the solution was allowed to rest for 4 to 5 hours to get a visually apparent phase separation of the bromine-poor aqueous phase and dark-coloured, bromine-rich polybromide phase. Orange-coloured or yellow-coloured aqueous phases were observed when using MEP or 3-MBPy, respectively whereas dark red-coloured polybromide phase was noted in both cases settled at the bottom of the tank.

A custom-made flow setup was developed for battery testing, as shown in Fig. 2b. To store the electrolytes, two polypropylene measuring cylinders of 200 mL and 50 mL capacity, respectively, were placed in a concentric arrangement, with the smaller cylinder elevated and with its bottom surface cut out. Aqueous phase of the electrolyte was directly drawn from the top side of this smaller cylinder using 2 mm PTFE tubing (BOLA, Bohlender, Germany) *via* 1/8″ Tygon tubing (Cole-Parmer, USA) and pumped into one side of the mixer using a peristaltic pump (Masteflex, Cole-Parmer, USA). The polybromide phase was drawn from the bottom of the larger cylinder reservoir and pumped using a PTFE tubing into the mixer using a second peristaltic pump. Both phases were then mixed well in a mixer compartment (5 cm × 5 cm × 3 cm) using a magnetic stirrer (Fried Electric, IL) with a cross-shaped magnetic bar for efficient mixing. This mixer was custom-made using our CNC milling machine from PVDF, had a 44 cm^3 internal capacity, separate inlets for aqueous and polybromide phases, and one outlet at the top. This outlet of mixer delivered the well-mixed emulsion electrolyte to the inlet of the cell. The battery was horizontally positioned battery with the zinc electrode side facing upwards and outlet of the battery was sent back to the reservoir using PTFE tubing. The complete experimental flow setup with battery, tank, pumps and mixer is illustrated in Fig. 2b.

During battery cycling measurement, volume fractions of aqueous and polybromide phases entering the mixer part were controlled by setting up the required flow rate in each peristaltic pump. For instance, in the case of a polybromide volume fraction, ψ, of 5%, the polybromide phase flow rate was set at 5 mL min^{-1} in pump 2 and aqueous phase flow rate was set at 95 mL min^{-1} in pump 1. Correspondingly, in the case of ψ = 1%, the polybromide phase flow rate was set at 1 mL min^{-1} in pump 2 and the aqueous phase flow rate was set at 99 mL min^{-1} in pump 1. The total electrolyte flow rate was constant (100 mL min^{-1}) for all the experiments, and ψ = 0% (only the aqueous phase) was used during charging.

The electrochemical and cycling experiments were performed at room temperature using a potentiostat/galvanostat in a two-electrode configuration (Gamry reference 3000, USA). Electrolyte *in situ* and *ex situ* ionic conductivity was measured for various electrolytes with initial (pre-partitioned) bromine concentrations ranging from 0.25 M to 2 M. The *in situ* investigation was carried out using galvanostatic electrochemical impedance spectroscopy (GEIS) with frequency ranges from 100 KHz to 100 mHz at zero DC current. A calibration constant of 1.8 was obtained by flowing a known conductivity electrolyte through the battery and measuring the high frequency intercept of the real axis on the Nyquist plot, which was then used to calculate the *in situ* electrolyte conductivity. The *ex situ* conductivity of the aqueous phase was measured using a conductivity meter (Thermo Scientific, Indonesia) corrected to 23 °C. A rheometric investigation of aqueous and polybromide phases with various initial bromine concentrations of 0.25 M to 2 M Br_2 was performed using an MRC 102 rheometer (Anton Paar, Austria) with a double-gap cylindrical geometry (DG 26.7, titanium) and RheoCompassTM software. For each electrolyte sample (4 mL), shear stress was measured over ten logarithmically spanned shear rate values in the range 500 to 50 s^{-1} and the averaged viscosity is presented, since all the samples were found to behave as Newtonian fluids. Bromine concentration in the aqueous phase after bromine partitioning, as a function of the pre-partitioned (initial) bromine concentrations added to the solution was measured by iodometric titration. All the battery and electrolyte characterization studies were carried out at room temperature.

The cycling experiments were performed with a 200 mL electrolyte batch containing 2 M $ZnBr_2$, 0.5 M Br_2, 0.5 M MEP or 3-MBPy at 0% state of charge (SOC) and circulated at a total flow rate of 100 mL min^{-1}. The charging was carried out at a constant current density of 30 mA cm^{-2} for 100 min to achieve a zinc loading of 50 mA h cm^{-2} (100% SOC), at which the Br_2 concentration increased to 0.55 M, the $ZnBr_2$ concentration correspondingly decreased to 1.95 M, and the expected Zn deposition thickness was 86 μm. The discharge at the same current density until the cell voltage dropped below 0.5 V. Each cycle was repeated for a total of 5 times while using the polybromide volume fraction ψ = 0% during the charging and ψ = 1% or 5% during the discharge.

3. Results and discussion

3.1. Electrolyte characterization

In order to gain insight into the electrolyte properties when using either weaker-binding MEP or stronger-binding 3-MBPy, we performed several fundamental *ex situ* characterization studies. An iodometric titration was conducted to analyze the concentration of bromine in the aqueous phase at equilibrium, and thus to quantify the binding strength of the BCA. The solution composition used was 2 M $ZnBr_2$, 0.5 M MEP or 3-MBPy, and an initial (pre-partitioning) bromine concentration varying from 0.25 M to 2 M. The bromine, once added to the electrolyte, partitioned between polybromide and aqueous phases, and the aqueous phase at equilibrium was taken and analyzed *via* iodometric titrations. As shown in Fig. 3a, aqueous bromine concentration increases with increasing bromine loading, as expected.[22,39] When using MEP, the measured bromine concentration of the aqueous phase at equilibrium for 0.25, 0.5, 0.75, 1, 1.25, 1.5, and 2 M initial bromine concentration was, respectively, 34, 39, 52, 77, 113, 177 and 375 mM.

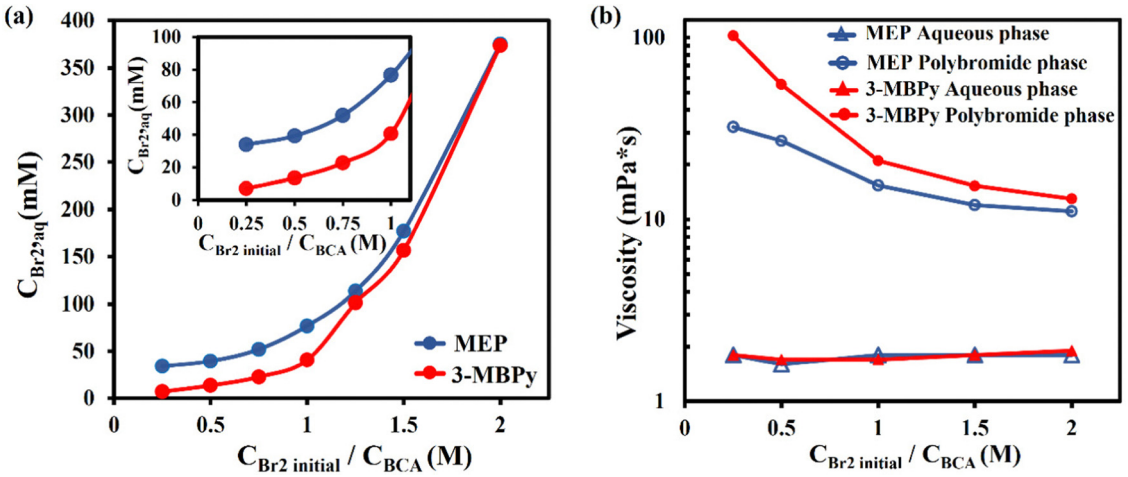

Fig. 3 *Ex situ* characterization of electrolytes containing initial (pre-partition) bromine concentration ranging from 0.25 M to 2 M, as well as 2 M $ZnBr_2$, and 0.5 MEP or 3-MBPy. (a) Measured bromine concentration in the aqueous phase at equilibrium, *versus* initial bromine concentration. (b) Measured viscosity of each phase *versus* initial bromine concentration.

Thus, aqueous phase bromine concentration was relatively stable at around 35 mM until the initial bromine concentration exceeded that of the MEP, above which the aqueous phase concentration rapidly increased with initial bromine concentration. For the case with 3-MBPy, we obtained instead 7, 14, 23, 41, 101, 157 and 373 mM respectively. For nearly each tested initial bromine concentration, the aqueous phase when using MEP shows a higher bromine concentration than when using 3-MBPy. At initial bromine concentration of 0.5 M, the aqueous phase when using MEP was at 39 mM while that when using 3-MBPy was nearly three-fold lower at 14 mM. Thus, we conclude that 3-MBPy shows significantly stronger binding with bromine than MEP. This is expected because 3-MBPy has a longer alkyl side chain than MEP (butyl *vs.* ethyl);[40] however to our knowledge this is the first characterization of the aqueous phase bromine concentration of emulsive battery electrolytes using 3-MBPy. We further consider the low aqueous-phase concentration of bromine obtained when using 3-MBPy to be promising towards reduced zinc corrosion during battery cycling and enhanced coulombic efficiency.

Electrolyte viscosity can play an important role in the flow battery performance and choice of operational parameters. For the case of an emulsive electrolyte, there is a potential risk for relatively high flow viscosity, resulting in excessive pumping losses or channel clogging. Furthermore, emulsions may behave as non-Newtonian fluids,[41] complicating the effect of electrolyte viscosity on the battery performance due to strong variations in shear rates within the battery flow channel. We measured the viscosity of each phase of our electrolyte *versus* shear rate *via* a rheometer, for an electrolyte composed of 2 M $ZnBr_2$, 0.5 M MEP or 3-MBPy, and initial Br_2 concentrations ranging from 0.25 M to 2 M. From the results in Fig. 3b, the aqueous phase viscosities of the electrolyte containing MEP or 3-MBPy were nearly analogous, both showing between ~1.7 and 1.9 mPa s viscosity and with largely Newtonian (shear-independent) behavior (see S1, ESI†). This indicates that increasing the aqueous phase bromine concentration, even by an order of magnitude (see Fig. 3), has no significant effect on the aqueous phase viscosity. The measured viscosities of polybromide phase also demonstrate Newtonian behavior with largely shear-independent viscosity (S2, ESI†), but the viscosity is generally at least an order of magnitude higher than that of the aqueous phase. Here, we find that initial bromine concentration is crucial in determining the viscosity of the polybromide phase, where generally increasing bromine concentration results in reduced viscosity. Furthermore, although the viscosity of the polybromide phase with 3-MBPy is about three times more viscous that that of MEP at 0.25 M Br_2, 102.3 as compared to 32.3 mPa s, the viscosities converge to nearly the same value as initial Br_2 concentration increases, to just over 10 mPa s. The latter observations may be because, in the polybromide phase, the Br_2 molecules exist as polybromide anions Br_3^-, Br_5^-, Br_7^-, Br_9^- balanced by the organic cations, in our case – $[3\text{-MBPy}]^+$ or $[MEP]^+$. The predominant anion shifts from Br_3^- towards Br_7^- as the initial Br_2 concentration in the electrolyte increases from 0.25 M to 2 M.[21] The binding strength of the BCA cation towards higher polybromides is weaker than that towards lower polybromides, as explained by DFT studies,[24] and less dependent on the BCA type.[21] As a result, the viscosity of the polybromide phase decreases with the increasing initial Br_2 concentration and the difference between the 3-MBPy polybromide phase and the MEP polybromide phase diminishes.[40]

In battery applications, electrolyte ionic conductivity is an important parameter which often determines battery Ohmic losses and has a strong impact on voltage efficiency. For *ex situ* conductivity measurements, shown in Fig. 4a, equilibrated solutions of 2 M $ZnBr_2$, 0.5 M MEP or 3-MBPy and with various initial bromine concentrations from 0.25 M to 2 M were used. This measurement was carried out on the aqueous phase alone (ψ = 0%), and the resulting conductivity values were compared to a 2 M $ZnBr_2$ solution of ~114 mS cm^{-1} (dashed green line). It can be observed in Fig. 4a that the addition of BCA reduces

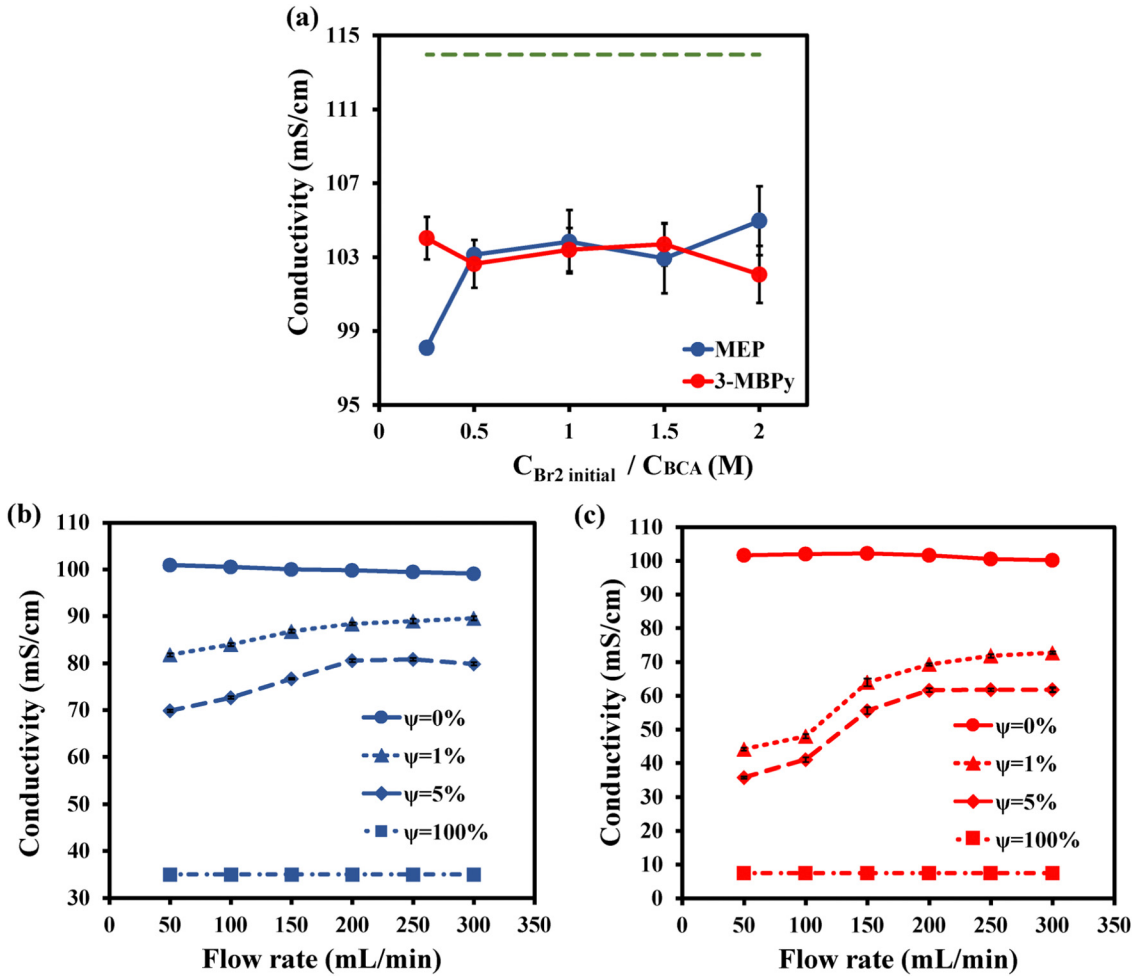

Fig. 4 *Ex situ* and *in situ* characterizations of electrolyte ionic conductivity when containing initial (pre-partition) bromine concentration ranging from 0.25 M to 2 M, as well as 2 M $ZnBr_2$, and 0.5 MEP or 3-MBPy. (a) *Ex situ* conductivity measurements of the aqueous phase alone with reference to that of a 2 M $ZnBr_2$ solution (dashed green line), (b) *in situ* conductivity measurements for ψ = 0%, ψ = 1%, ψ = 5%, and ψ = 100% *versus* electrolyte flow rate and for an initial bromine concentration of 0.5 M Br_2 and 0.5 MEP. (c) The same measurements as in (b) except for 3-MBPy as a complexing agent.

ionic conductivity of the electrolyte below that of the pure $ZnBr_2$ solution, as has been previously observed.[42] Kuttinger *et al.* observed a decrease in the conductivity of pure HBr electrolyte with the addition of BCA.[21] Conductivity of the aqueous phase mainly depends on the nature of the $[BCA]^+$ cation. At low bromine concentration, the $[3\text{-MBPy}]^+$ cation having a long alkyl side chain leads to a decrease in conductivity likely due to increasing solution viscosity.[21] Both MEP and 3-MBPy show gradual increase in conductivity with increasing bromine concentration. This is likely because at high bromine concentration, $[BCA]^+$ cations are bonded to the polybromide phase and thus removed from the aqueous phase.[39] It was observed that when using either MEP or 3-MBPy, there was not much change in the measured aqueous phase conductivity. For 0.5, 1 and 1.5 M bromine concentrations, the measured conductivity was 103, 103 and 104 mS cm^{-1} for electrolytes with MEP, and 103, 104 and 103 mS cm^{-1}, respectively, for 3-MBPy.

Electrolyte *in situ* conductivity was evaluated from GEIS measurements and extracting the high frequency intercept of the impedance of the battery cell at various flow rates. Four distinct electrolyte polybromide volume fractions were studied, including ψ = 0% (only aqueous phase), ψ = 1%, ψ = 5%, and ψ = 100%, for flow rates ranging from 50 mL min^{-1} to 300 mL min^{-1}. The initial, pre-complexation electrolyte included 2 M $ZnBr_2$ 0.5 M Br_2 and 0.5 M MEP or 3-MBPy, and the corresponding conductivity values were graphically shown in Fig. 4b for MEP and Fig. 4c for 3-MBPy. For ψ = 0% and 100%, the measured conductivity was not significantly affected by flow rate. Conductivity value of the polybromide phase (ψ = 100%) of 3-MBPy was four-fold lower than the MEP polybromide phase. At lower flow rates, the measured conductivity at ψ = 1% and 5% is significantly lower for 3-MBPy, showing the role of stronger complexing properties towards bromine, which makes the total polybromide phase denser and viscous, resulting in decreased conductivity compared to MEP. As can be seen, the *in situ* and *ex situ* conductivity values of the aqueous phase for MEP and 3-MBPy (ψ = 0%) are nearly identical. Increasing the polybromide volume fraction significantly increases the polybromide layer thickness and hence decreasing the conductivity. Besides, gravity and mixing conditions

play a vital role in determining the electrolyte conductivity at a low flow rate and high polybromide volume fraction.[35] At high flow rates exceeding 250 mL min^{-1}, the measured electrolyte conductivity values by Ronen *et al.*[35] at ψ = 5% with MEP are higher ($\sim$95 mS cm^{-1}) than that obtained here (77 mS cm^{-1}) for ψ = 5% with MEP. This is likely due to differences in emulsion mixing conditions, since the latter authors used a conventional overhead mixer with a perforated bar for stirring the electrolyte, as compared to the use of a magnetic mixing bar used here (Fig. 2b). A more vigorous mixing employed by Ronen *et al.* likely resulted in smaller polybromide droplet size in the electrolyte, and reduced polybromide sedimentation, illustrating the potential strong effect of upstream mixing conditions on battery polybromide distributions.

3.2. Flow battery characterization

Galvanostatic charge–discharge of the battery cell was carried out to investigate voltage (VE), coulombic (CE) and energy battery efficiency. A typical charge–discharge curve for electrolytes with ψ = 1% and 5% are displayed in Fig. 5a and b, where the first cycle performance was plotted out of five cycles. As shown in Fig. 5a for ψ = 1%, the average charge voltage plateau is 1.93 and 1.90 for MEP and 3-MBPy respectively, while the average discharge voltage plateau for MEP starts at 1.46 V and for 3-MBPy at 1.55 V. Moreover, when using MEP as a complexing agent, discharging lasted for up to 47.5 min, whereas with 3-MBPy, 69.5 min was obtained. Similarly, at ψ = 5%, the cell using 3-MBPy lasted for 57 min during discharging, 19 minutes higher than MEP. This longer discharge time is due to reduced zinc corrosion during cycling with 3-MBPy, a result of the reduced aqueous-phase bromine concentration when using a stronger-binding complexing agent.

From Fig. 5a and b, the cycles VE and CE can be calculated, and these are shown in Fig. 5c. At ψ = 1% and when using MEP, a CE of 47% is attained, with 3-MBPy, CE is further improved to 69%. This demonstrates that CE of the single-flow battery

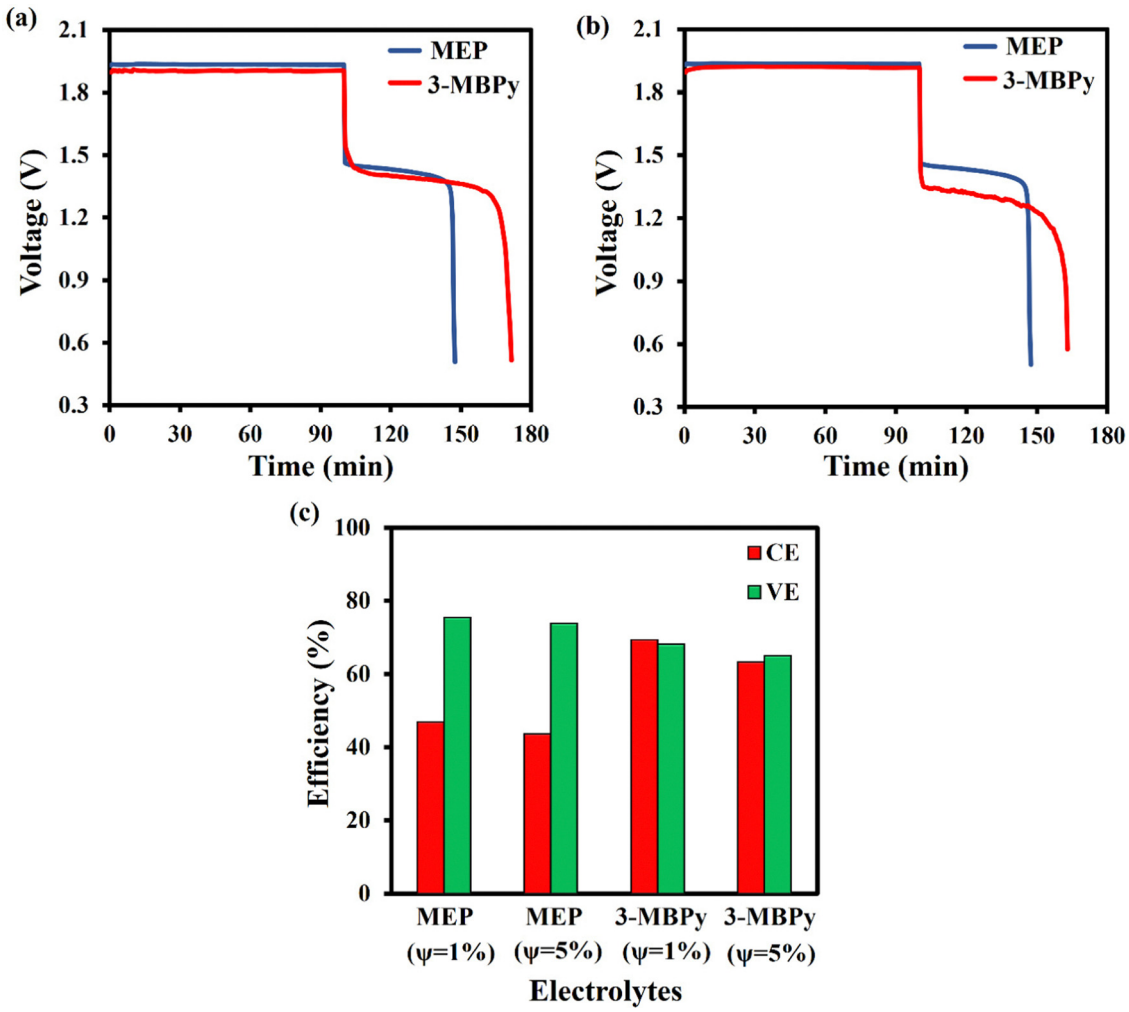

Fig. 5 The performance of the prototype single-flow battery cell with either MEP or 3-MBPy complexing agent when charged from 0% SOC to 100% SOC: (a) a representative galvanostatic charge–discharge profile with MEP or 3-MBPy for ψ = 1% and at a current density of 30 mA cm^{-2}. (b) The same measurement but for ψ = 5%, and (c) tabulated coulombic efficiency (CE), voltage efficiency (VE), for electrolytes with MEP or 3-MBPy and either ψ = 1% or ψ = 5%.

leveraging multiphase flow can be substantially improved by using a stronger-binding complexing agent. Although the CE remains too low for practical application, uncovering this important pathway to CE improvement opens the door for yet-further improvements in the future. The corresponding VEs when using MEP or 3-MBPy as complexing agents were 70% and 68%, respectively. 3-MBPy exhibits slightly lower VE than MEP, likely because of the poorer conductivity of its viscous polybromide phase, which may have settled somewhat onto the cathode.[35] On the other hand, at ψ = 5%, 3-MBPy displays maximum CE and VE of 63% and 65% whereas MEP displays maximum of 43% CE and 64% VE respectively. Because of the high viscosity and low conductivity, increasing the polybromide volume fraction slightly reduces the CE and VE. However, high polybromide volume fraction might be vital at a high loading capacity. The main observation here is that at ψ = 5% CE and VE are slightly decreased compared to ψ = 1%.

4. Conclusions

In summary, this work introduces the complexing agent 3-MBPy for use in a single-flow zinc–bromine battery with a multiphase flow electrolyte and compares it to the widely used complexing agent MEP. Iodometric titration showing a three-fold decrease in the bromine concentration in the aqueous phase when using a stronger-binding complexing agent (3-MBPy) than MEP. The former leads to reduced zinc corrosion during battery cycling, and a 23% increase in the CE. This gain in CE demonstrates that such single-flow and membraneless batteries can be realized in practice using stronger-binding complexing agents. In future, the cycling efficiencies can be further enhanced by modifications to the battery design to minimize settling and management of the polybromide phase within the cell, as well as to optimize the multiphase flow profile.

Conflicts of interest

There are no conflicts to declare.

Acknowledgements

The authors would like to thank the Nancy and Stephen Grand Technion Energy program (GTEP), and Israel Science Foundation (ISF, 3191/21) for its financial support.

References

1 A. Demirbas, A. Sahin-demirbas and A. Hilal Demirbas, *Energy Sources*, 2004, **26**, 191–204.
2 E. Samerón Manzano, A. J. Perea-Moreno and M. A. Perea-Moreno, *Sustainability*, 2019, **11**, 863.
3 L. Li, Z. Yang, W. Wang, Q. Luo, B. Li and X. Wei, *Adv. Funct. Mater.*, 2013, **23**, 970–986.
4 Q. Ma, X. X. Zeng, C. Zhou, Q. Deng, P. F. Wang, T. T. Zuo, X. D. Zhang, Y. X. Yin, X. Wu, L. Y. Chai and Y. G. Guo, *ACS Appl. Mater. Interfaces*, 2018, **10**, 22381–22388.
5 Y. K. Zeng, X. L. Zhou, L. An, L. Wei and T. S. Zhao, *J. Power Sources*, 2016, **324**, 738–744.
6 Z. Li, G. Weng, Q. Zou, G. Cong and Y. C. Lu, *Nano Energy*, 2016, **30**, 283–292.
7 H. Zhou, H. Zhang, P. Zhao and B. Yi, *Electrochim. Acta*, 2006, **51**, 6304–6312.
8 R. Ronen, A. D. Gat, M. Z. Bazant and M. E. Suss, *Electrochim. Acta*, 2021, **389**, 138554.
9 G. Nikiforidis, L. Berlouis, D. Hall and D. Hodgson, *J. Power Sources*, 2012, **206**, 497–503.
10 P. Bai and M. Z. Bazant, *Electrochim. Acta*, 2016, **202**, 216–223.
11 Y. Zhao, Y. Ding, Y. Li, L. Peng, H. R. Byon, J. B. Goodenough and G. Yu, *Chem. Soc. Rev.*, 2015, **44**, 7968–7996.
12 F. Pan and Q. Wang, *Molecules*, 2015, **20**, 20499–20517.
13 F. C. Wals., C. Ponce Leon, A. Frıas-Ferrer, J. Gonzalez-Garcia and D. A. Szanto, *J. Power Sources*, 2006, **160**, 716–732.
14 M. Schneider, G. P. Rajarathnam, M. E. Easton, A. F. Masters, T. Maschmeyer and A. M. Vassallo, *RSC Adv.*, 2016, **6**, 110548–110556.
15 A. M. Lackner, R. C. Knechtli. and H. S. Lim, *J. Electrochem. Soc.*, 1977, **124**, 1154.
16 D. Linden and T. B. Reddy, *Handbook of batteries*, 1995, vol. 33.
17 Y. Yin, Z. Yuan and X. Li, *Phys. Chem. Chem. Phys.*, 2021, **23**, 26070–26084.
18 A. Khor, P. Leung, M. R. Mohamed, C. Flox, Q. Xu, L. An, R. G. A. Wills, J. R. Morante and A. A. Shah, *Mater. Today Energy*, 2018, **8**, 80–108.
19 Z. Xu, Q. Fan, Y. Li, J. Wang and P. D. Lund, *Renewable Sustainable Energy Rev.*, 2020, **127**, 109838.
20 J. D. Jeon, H. S. Yang, J. Shim, H. S. Kim and J. H. Yang, *Electrochim. Acta*, 2014, **127**, 397–402.
21 M. Küttinger, P. A. Loichet Torres, E. Meyer, P. Fischer and J. Tübke, *Molecules*, 2021, **26**, 2721.
22 D. C. Constable, P. M. Hoobin, K. J. Cathro and K. Cedzynska, *J. Power Sources*, 1986, **18**, 349–370.
23 D. J. Eustace, *J. Electrochem. Soc.*, 1979, **79–2**, 290–294.
24 M. E. Easton, A. J. Ward, B. Chan, L. Radom, A. F. Masters and T. Maschmeyer, *Phys. Chem. Chem. Phys.*, 2016, **18**, 7251–7260.
25 H. Kamath, S. Rajagopalan and M. Zwillenberg, EPRI, Palo Alto.
26 M. E. Suss, K. Conforti, L. Gilson, C. R. Buie and M. Z. Bazant, *RSC Adv.*, 2016, **6**, 100209–100213.
27 A. Z. Weber, M. M. Mench, J. P. Meyers, P. N. Ross, J. T. Gostick and Q. Liu, *J. Appl. Electrochem.*, 2011, **41**, 1137–1164.
28 W. A. Braff, M. Z. Bazant and C. R. Buie, *Nat. Commun.*, 2013, **4**, 1–6.
29 D. Alfisi, A. N. Shocron, R. Gloukhovski, D. A. Vermaas and M. E. Suss, *ACS Sustainable Chem. Eng.*, 2022, **10**, 12985–12992.
30 Q. Lai, H. Zhang, X. Li, L. Zhang and Y. Cheng, *J. Power Sources*, 2013, **235**, 1–4.
31 S. Biswas, A. Senju, R. Mohr, T. Hodson, N. Karthikeyan, K. W. Knehr, A. G. Hsieh, X. Yang, B. E. Koel and D. A. Steingart, *Energy Environ. Sci.*, 2017, **10**, 114–120.

32 J. H. Lee, Y. Byun, G. H. Jeong, C. Choi, J. Kwen, R. Kim, I. H. Kim, S. O. Kim and H. T. Kim, *Adv. Mater.*, 2019, **31**, 1904524.
33 S. Liu, J. Wu, J. Huang, X. Chi, J. Yang and Y. Liu, *Sustainable Energy Fuels*, 2022, **6**, 1148–1155.
34 L. Amit, D. Naar, R. Gloukhovski, G. J. la O' and M. E. Suss, *ChemSusChem*, 2021, **14**, 1068–1073.
35 R. Ronen, R. Gloukhovski and M. E. Suss, *J. Power Sources*, 2022, **540**, 231567.
36 J. Peng, N. M. Cantillo, Y. Xiao, K. M. Nelms, L. S. Roberts, G. Goenaga, A. Imel, B. A. Barth, M. Dadmun, D. G. Hayes and T. Zawodzinski, *J. Electrochem. Soc.*, 2021, **168**, 080502.
37 X. Shen, N. Sinclair, J. Wainright, A. Imel, B. Barth, T. Zawodzinski and R. F. Savinell, *J. Electrochem. Soc.*, 2021, **168**, 060539.
38 B. A. Barth, A. Imel, K. M. K. Nelms, G. A. Goenaga and T. Zawodzinski, *Front. Chem.*, 2022, **10**, 1–12.
39 M. Küttinger, R. Riasse, J. Wlodarczyk, P. Fischer and J. Tübke, *J. Power Sources*, 2022, **520**, 230804.
40 M. Küttinger, P. A. Loichet Torres, E. Meyer and P. Fischer, *Chem. – Eur. J.*, 2022, **28**, e202103491.
41 D. Dan and G. Jing, *J. Pet. Sci. Eng.*, 2006, **53**, 113–122.
42 I. B. David, M. Freiberg, E. Lancry and B. Z. Magnes, *ECS Trans.*, 2013, **53**, 107–115.